Chalcogenide Letters Vol. 17, No. 4, April 2020, p. 187 - 196

GAMMA RAY SHIELDING PARAMETER OF BARIUM-BORO-TELLURITE GLASS

A. AZURAIDA[a,*], M. K. HALIMAH[b], M. ISHAK[c], L. HASNIMULYATI[d], S. I. AHMAD[a]

[a]*Physics Department, Centre for Defence Foundation Studies, Universiti Pertahanan Nasional Malaysia, 57000 Sungai Besi, Kuala Lumpur, Malaysia*
[b]*Physics Department, Faculty of Science, Universiti Putra Malaysia, 43400 UPM Serdang, Selangor, Malaysia*
[c]*Malaysia Nuclear Agency, 43000, Bangi, Kajang, Selangor, Malaysia*
[d]*Physics Department, Faculty of Applied Sciences, Universiti Teknologi MARA Cawangan Pahang, Kampus Jengka, 26400 Jengka, Pahang, Malaysia*

Boro-tellurite glasses have recently been attracting the attention of several researchers as a tremendous optical device and shielding material. In this work, we have synthesized boro-tellurite glasses with barium oxide (BaO) by melt quenching technique. The structural and shielding property changes after adding of barium oxide in boro-tellurite glass were studied using Fourier Transform Infrared (FTIR) and Lead Equivalent Thickness measurement (LET), respectively. The results show that the bismuth oxide increases glass density, changes the glass structure, and increases the radiation shielding properties. Changes in the glass structure are due to atomic rearrangements and formation of non-bridging oxygen (NBO). The density of boro-tellurite glass system increased when BaO content increased, which is due to the high molecular weight of BaO and the increasing number of non-bridging oxygen (NBO) atoms in the glass structure. In addition, the mass attenuation coefficient, μ_m of the glass system increases as BaO concentration increases and the half value layer, HVL and mean free path, MFP of 30BaBTe glass is better than some standard concretes.

(Received October 24, 2019; April 6, 2020)

Keywords: Boro-tellurite, Barium, Gamma radiation shielding properties

1. Introduction

Gamma radiation sources which are obtained from radioisotopes have a high potential to be harmful to human health and also can damage sensitive laboratory equipment. Therefore, a high quality shielding material is required to attenuate the radiation to safety and acceptable levels. Tiles, concrete blocks, and clay bricks are traditional materials used for radiation shielding. However, the use of transparent materials such as glass is very important as a shielding material especially for viewing windows in doors to radiation areas.

For a few decades, there are various types of glass development by scientists and researchers to produce high-quality radiation shielding glass such as phosphate-, silicate-, borate- and tellurite-based glass. Most of the glasses are added with lead because it has heavy mass and it can produce high density glass. Previous works [1-3] reported that the addition of different concentrations of lead oxide in borate glass produced high density glass up to 5 gcm-3, and proven as a transparent radiation shielding material. However, the use of lead can cause several undesirable effects such as weakness, anemia, miscarriages and kidney and brain damage. Very high lead exposure can cause death. The International Agency for Research on Cancer (IARC) and The Department of Health and Human Services (DHHS) have determined that lead and lead compounds causes environmental toxic and probably carcinogenic to humans. Because of the aforementioned effects, barium can be used in replacing lead for the development of a radiation

* Corresponding author : azuraida@upnm.edu.my

shielding material. Barium is not carcinogenic, non-poison and it does not bio–accumulate [4]. Singh et al., (2002) reported that barium-borate glasses have good value in mass attenuation coefficient and effective atomic number, which make good radiation shielding materials [5]. Kaur et al., (2019) observed that barium in $65Bi_2O_3 - xBaO - (35 - x)B_2O_3$ glass system plays the role of a modifier and it is responsible for conversion of triangular [BO_3] units to tetrahedral [BO_4] units along with formation of non-bridging oxygen and increase in ionic character [6]. It also increases the radiation shielding abilities of the glass system at 662 keV energy. In addition, the presence of more heavily doped elements like barium in the glass system led them to exhibit better shielding properties which can be utilized as replacement materials for concrete and lead based glasses as efficient shielding materials [7].

Current work aims to synthesize transparent radiation shielding glasses modified with barium element. This paper will report the effects of barium in a boro-tellurite glass system which concentrates on two properties: (i) physical and structural properties, and (ii) gamma radiation shielding properties. Boro-tellurite was chosen as a base glass in this research because of its unique characteristics such as high transparency, good gamma shielding properties and high thermal resistance when added with heavy metal oxides [8]. It is expected that the addition of barium oxide in boro-tellurite glass would increase the glass density and improve the gamma radiation shielding properties.

2. Experimental procedure

2.1. Materials and glass preparation

$[(TeO_2)_{0.7}(B_2O_3)_{0.3}]_{1-x}(BaO)_x$ glass system with x = 0.00, 0.05, 0.10, 0.15, 0.20, 0.25 and 0.30 mole fraction were prepared by using a conventional melt quenching method. The chemicals from Assay, Alfa Aesar such as tellurium (IV) dioxide (TeO_2), boron oxide (B_2O_3) and barium oxide (BaO) were mixed together and manually ground (about 20 minutes) using an agate mortar. The mixture was then preheated at 350 °C and then melted at 900 °C using an electrical furnace. The molten glass was quenched in air at room temperature by pouring it into a preheated stainless steel cylindrically shaped mould and annealed at 400 °C. After one hour of annealing process, the furnace was turned off and the glass samples were allowed to cool down to room temperature.

2.2. Density and structural analysis

Glass density, ρ_g, was measured using the Archimedes principle. Distilled water (density = 1.00 g cm^{-3}) was used as the immersion liquid. The weight of each bulk glass was measured in air and distilled water using a densitometer. The glass density was determined using the relation

$$\rho_g = \frac{W_a}{W_a - W_d}\rho_d \quad (1)$$

where W_a is the weight of glass in air, W_d is the weight of glass in distilled water and ρ_d is the density of distilled water.

The molar volume, V_m is the volume occupied by one mole of a substance from chemical element or chemical compound at a given temperature and pressure. The molar volume of a glass can be obtained by relation:

$$V_m = \left(\frac{M}{\rho}\right) \quad (2)$$

where M is molecular weight of the substances and ρ is the density of glass sample.

A small part from each glass samples was crushed and ground to form powder for X-ray Diffractometer (XRD) analysis and Fourier Transform Infrared (FTIR). The amorphous nature of all glass samples was observed from XRD analysis using an X-ray Diffractometer (PAnalytical Philips) X'Pert Pro PW 3040/60) in the 2θ range 20°- 80°. FTIR spectroscopy was used to identify the structural bonding of the glass at room temperature. The FTIR spectrum was recorded in the range from 220 to 4000 cm^{-1}.

2.3. Shielding parameters measurement

Gamma ray attenuation for glass samples were performed using lead equivalent thickness measurement setup with gamma emitting source from cesium-137 (Cs-137). The geometry diagram for this measurement is shown in Figure 1. The symmetry axis of the arrangement is a horizontal line adjusted by a laser beam. The Cs-137 source was enclosed with 5 mm width lead container are placed 100 cm from sample. Glass samples with different thicknesses of 20 – 150 mm were arranged between two collimators, which have 0.5 and 1.5 mm apertures for each collimator. Both collimators are used to minimize the detection of any radiation coming directly from the source and scattered from the surroundings.

The reading of incident, Io and transmitted, I intensity of gamma ray from Cs-137 source through sample were detected using HPGe detector and recorded by Ludlum scaler rate meter Model 220. The I_o and I reading were recorded for 1 minute and repeated a minimum of 10 times for each glass samples. With that, linear attenuation coefficients can be obtained from the slope of plot In (I_o/I) versus glass thickness. The linear attenuation coefficient values was then used to calculate mass attenuation coefficient, μ_m and other shielding parameters such as, half value layer and mean free path.

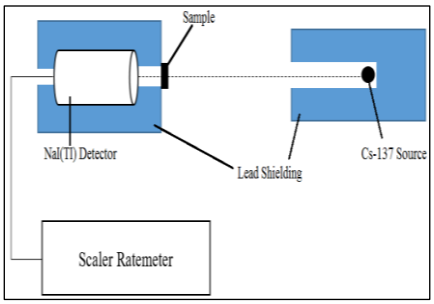

Fig. 1. Geometrical diagram for Lead Equipment Thickness (LET) measurement.

The relation between initial intensity radiation, I_o and attenuated radiation through any medium (sample), I can be expressed as:

$$I = I_o \exp[-\mu t] \tag{3}$$

where μ is linear attenuation coefficient, ρ is density of sample and t is thickness of sample.

In order to quantify the attenuation of a material which is independent of density, the mass attenuation coefficient (μ/ρ) is being used by providing thicknesses in mass per unit area (ρt) in (g/cm^2), where ρt is known as mass thickness or areal thickness of the absorbing material.

Half value layer, HVL is the convenient parameter to represent gamma ray interaction of a material. The HVL is the thickness of particular material needed to reduce the intensity of gamma ray to half of its initial value. The half value layer value can be calculated by following relation:

$$HVL = \frac{0.693}{\mu} \tag{4}$$

While, mean free path, MFP corresponds to the average distance travelled by a moving particle (atom/molecule/photon) between two consecutive collisions. It can be calculated by using equation:

$$MFP = \frac{1}{\mu_m \rho} \tag{5}$$

3. Results and discussion

3.1. Physical properties

The density of glass can be explained as the degree of change in various structural units in the glass composition. Generally, glass which contains heavy metal oxide will produce a high density glass. Table 1 shows seven glasses with different amounts of BaO. All of the glasses were transparent and free of air bubbles. They show different color tones from colorless to light-green color depending on the BaO percentage.

Table 1. Boro-Tellurite glass samples and densities.

No	Sample	Mole fraction BaO	Density, ρ (gcm^{-3})	Molar volume, V_m ($cm^3\ mol^{-1}$)
1	BTe	0	3.17	40.86
2	5BaBTe	0.05	3.28	39.97
3	10BaBTe	0.10	3.38	39.85
4	15BaBTe	0.15	3.46	39.31
5	20BaBTe	0.20	3.56	39.14
6	25BaBTe	0.25	3.59	38.43
7	30BaBTe	0.30	3.63	38.20

Fig. 2 depicted the density and molar volume against BaO concentration. The densities are increased from 3.17 gcm^{-3} to 3.63 gcm^{-3} while the molar volume decreased from 40.86 $cm^3\ mol^{-1}$ to 38.20 $cm^3\ mol^{-1}$ as BaO content increased. The trend of this result follow the relationship between density and molar volume as shown in Equation 2, i.e the density and molar volume inversely proportional to each other. The density of this glass series increased by ~14% from 3.17 gcm^{-3} to 3.63 gcm^{-3} and the molar volume decreased by ~7% from 40.86 $cm^3\ mol^{-1}$ to 38.20 $cm^3\ mol^{-1}$. As expected, the small increment of glass density is due to the replacement of lower density of TeO_2 (5.67 gcm^{-3}) and B_2O_3 (2.46 gcm^{-3}) compared to BaO (5.72 gcm^{-3}). Manikandan *et al.*, (2012) stated that the BaO has a tendency to strengthen the three-dimensional nature of the glass network and made the glass more dense [9]. The density in the present work also closed with the density value of $0.4BaO\text{-}0.6B_2O_3$ glass (3.38 gcm^{-3}) [10] and $35.8BaO\text{-}64.2B_2O_3$ (3.61 gcm^{-3}) [11]. Desirena *et al.*, (2009) also had reported that the density of $20BaO–10Cs_2CO_3–70TeO_2$ glass is 4.733 gcm^{-3} [12], which is higher than the density observed in this work. The decreasing of molar volume may caused by a decreasing of bond length and a space between atoms in a glass network. This process then effects the compaction of glass network.

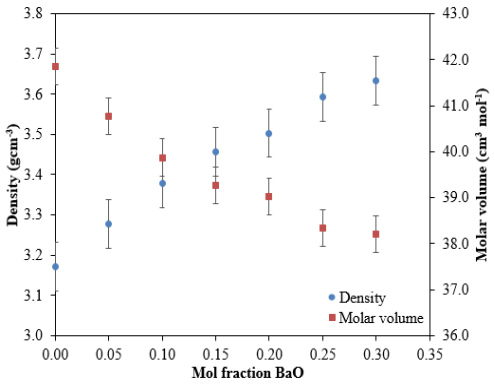

Fig. 2. Variation of density and molar volume for $[(TeO_2)_{0.7}(B_2O_3)_{0.3}]_{1-x}(BaO)_x$ glass system

3.2. Structural properties

Fig. 3 shows the X-ray diffraction pattern for $[(TeO_2)_{0.7}(B_2O_3)_{0.3}]_{1-x}(BaO)_x$ glasses. It is noted that the graph patterns are almost identical for all glasses. There is no sharp peak represents any crystal structure in the XRD spectra. This graph only shows the presence of a broad halo around $2\theta \cong 24\text{-}30^{\circ}$. Similar pattern of XRD graph also shown in multicomposition borotellurite glasses which was reported before. The absence of a sharp peak indicates that there is no long range order in atomic arrangements and this confirmed that all glass samples in this work are in an amorphous nature [13].

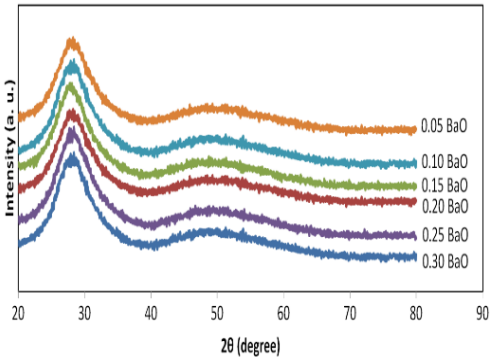

Fig. 3. XRD spectra for all glasses

FTIR analysis was performed to examine the distribution of structural bonding present in the studied glasses. The changes of FTIR spectra of all glasses are shown in Figure 4. The absorption peaks observed around 3600 cm^{-1} is attributed to O-H stretching vibrations [14], which commonly occur in oxide glass due to water entrapment of raw materials from the ambient atmosphere [8]. From Figure 4, the FTIR spectra of boro-tellurite (0BaO) glass exhibited two broad absorption peak centers at 1200 cm^{-1} and 1300 cm^{-1}, and two small intensity peaks at ~450 cm^{-1} and ~589 cm^{-1}. These peaks are almost similar to previous research for tellurite- [15] and borate-based [16] glass systems. The broad peak center at 1200 cm^{-1} was attributed to asymmetric stretching of B-O bonds from BO_4 tetrahedral and orthoborate groups, while another broad peak center at 1300 cm^{-1} are corresponding to the asymmetric stretching vibrations of B-O in the BO_3 unit with non-bridging oxygen from orthoborate, metaborate and pyroborate groups [17-18]. The small peak at ~450 $cm^{-1,}$ assigned to the linkage bending vibrations of Te-O-Te or O-Te-O [19], and ~589 cm^{-1} occurred due to vibrations of the Te-O bonds between TeO_4 and bridging oxygen [20].

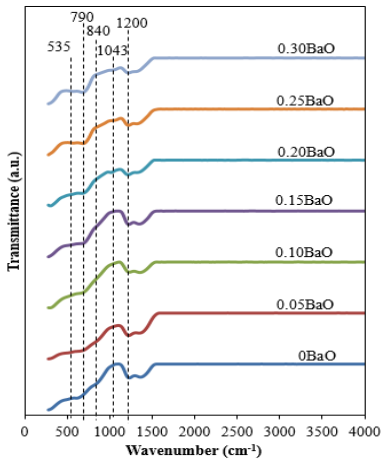

Fig. 4. FTIR spectra for all glasses

The FTIR spectra of $[(TeO_2)_{0.7}(B_2O_3)_{0.3}]_{1-x}(BaO)_x$ glass with x = 0 (0BaO) revealed two broad absorption peak centers at 1300 cm^{-1} and 1200 cm^{-1}, and two peaks with small intensity at ~589 cm^{-1} and ~450 cm^{-1}. The aforementioned peaks are almost similar with previous work for borate - and tellurite-based glass systems as reported by Sadeek *et al*., (2015) [16] and Sidek *et al*., (2009) [15], respectively. The broad peak center at 1300 cm^{-1} is attributed to the asymmetric stretching vibrations of B-O in the BO_3 unit with non-bridging oxygen from orthoborate, metaborate and pyroborate groups [21]. While the broad peak center at 1200 cm^{-1} was corresponding to asymmetric stretching of B-O bonds from BO_4 tetrahedral and orthoborate groups. The first small peak at ~589 cm^{-1} is assigned to the vibrations of Te-O bonds between TeO_4 and bridging oxygen, and second small peak at ~450 cm^{-1} is due to the linkage bending vibrations of Te-O-Te or O-Te-O [8,18].

The obtained FTIR specta for $[(TeO_2)_{0.7}(B_2O_3)_{0.3}]_{1-x}(BaO)_x$ glass system with x = 0.05 to 0.30 as plotted in Figure 4 exhibit two broad absorption band centers at 1300 cm^{-1} and 1200 cm^{-1}, three peaks with minor intensity at ~1043 cm^{-1}, 535 cm^{-1} and ~430 cm^{-1} and band shoulder at 790 cm^{-1}. Before the addition of BaO, the intensity of absorption band centers at 1300 cm^{-1} and 1200 cm^{-1} are almost similar. However, the band centers at 1300 cm^{-1} is decreased slowly while band centers at 1200 cm^{-1} increased (double compare initial) followed by the appearance of new absorption peak in range 840 – 1200 cm^{-1} as the BaO increased to maximum amount. The intensity of band (at 1200 cm^{-1}) increases with BaO concentration can be assigned to the increasing of B–O bond stretching vibration in the BO_3 unit from varied types of borate groups. While the appearance of new absorption peak are attributed to the existence of BO_4 absorption that agreed with the previous works reported by Kamitsos and Chryssikos (1991) [22], Khaled *et al*., (1994) [23] and Paz *et al*., (2016)[24]. The small absorption peak at 1043 cm^{-1} are due to stretching vibration of B-O bond from tetrahedral and peak occur near 535 cm^{-1} due to B-O-B vibration overlap with TeO_4 polyhedron. The observed of shoulder band at 790 cm^{-1} is assigned to stretching vibration of B-O-B in B_3O_6 boroxol rings overlap with Te-O bond with nonbridging oxigen. FTIR absorption band at 760-790 cm^{-1} in barium chloride-oxide tellurite glasses is contributed by three types of vibration: (i) Te=O double bond stretching vibration in $O_2Te=O$ groups, (ii) stretching vibrations of long Te-O bonds with nonbridging oxygen atoms in $O_3Te\text{-}O^-$ groups, and (iii) stretching vibrations of short Te-O bonds with nonbridging oxygen atoms in $O_3Te\text{-}O^-$ groups [25]. The assignments for each band for this glass series are shown in Tables 2.

The band position at ~430 cm^{-1} may be attributed to the bending and stretching of Te – O – Te and/or stretching of BO_4 units. The intensity of this band is found to decrease as BaO content increase. Decrement of band intensity may be related to increasing disruption of glass network effect the changes of bond lengths and/or bond angles. The low frequency of absorption band below 400 cm^{-1} also observed which due to the vibration of Ba^{2+} [26].

3.3. γ-ray shielding parameter

Lead equivalent thickness (LET) measurement were made to evaluate the linear attenuation coefficient, μ of glass sample. The LET measurement are using gamma ray from 137-cesium source. Intensity of incident (i) and transmitted (I) gamma ray through sample were used to evaluate linear attenuation coefficient, μ, and this value were used to calculate mass attenuation coefficient, μ_m value. Linear attenuation coefficient values are measured from the slope of linear graph Ln (I/i) against sample thickness, as shown in Figure 5. Another two γ-ray shielding parameter namely half value layer, HVL, and mean free path, MFP then also calculated by using μ and μ_m values.

Table 2. IR absorption band and band assignment of $[(TeO_2)_{0.7}(B_2O_3)_{0.3}]_{1-x}(BaO)_x$ glasses.

Wavenumber (cm^{-1})	Assignment of vibrational mode
1200 - 1300	B–O bond stretching vibration in the BO_3 unit from varied types of borate groups [24]
1043	stretching vibration of B-O bond from tetrahedral [26]
840	stretching vibrations of BO_3 units [27]
790	stretching vibration of B-O-B in B_3O_6 boroxol rings [25]
535	TeO_3 trigonal pyramid [28]
430	stretching of Te – O – Te units [28]
<400	vibration of Ba^{2+} [26]

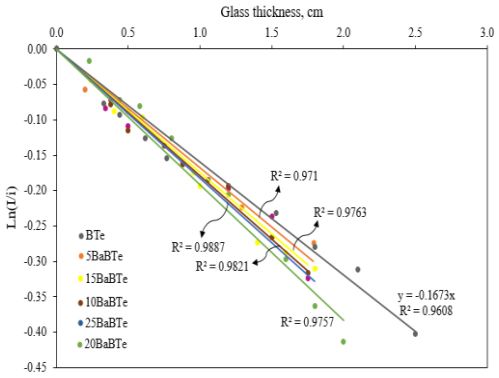

Fig. 5. Graph of Ln(I/i) against thickness of $[(TeO_2)_{0.7}(B_2O_3)_{0.3}]_{1-x}(BaO)_x$ glasses.

Fig. 5 shows the graph of Ln(I/i) against thickness of $[(TeO_2)_{0.7}(B_2O_3)_{0.3}]_{1-x}(BaO)_x$ glass system. The gradient from this graph which also known as linear attenuation coefficient, μ value are listed on the Table 3. It can be seen that the gradient of the graph is increased as barium content increase. This is due to higher atomic number of barium (56) rather than tellurium (52) and boron (5). As explained before, the density of glass modifier (Ba) also contributed in the increment of the μ value. However, the increment of the gradient of this glass system is small compared to a glass with bismuth content reported in previous work [14,29]. This because of: (i) atomic number of Bi (83) are much larger than Ba (56) and even larger than glass former (Te-52, B-5), and (ii) the density of Bi_2O_3 (8.9 gcm^{-3}) much higher than BaO (5.72 gcm^{-3}).

Table 3. Value of linear attenuation coefficient, μ, mass attenuation coefficient, μ_m , half value layer, HVL and mean free path, MFP for all glasses.

Glass	μ (cm^{-1})	μ_m (cm^2g^{-1})	HVL (cm)	MFP (cm)
BTe	0.1598	0.0459	4.763	6.873
5BaBTe	0.1673	0.0460	4.592	6.627
10BaBTe	0.1743	0.0462	4.474	6.456
15BaBTe	0.1787	0.0466	4.299	6.203
20BaBTe	0.1821	0.0476	4.239	6.116
25BaBTe	0.3218	0.0488	3.953	5.705
30BaBTe	0.3227	0.0491	3.988	5.234

Referring to Table 3, it is also observed that the increasing of BaO concentrations enhanced the mass attenuation coefficient, μ_m values. The highest μ_m value for $[(TeO_2)_{0.7}(B_2O_3)_{0.3}]_{1-x}(BaO)_x$ glass system is 0.0491 cm^2g^{-1}. As expected, the maximum concentration for each modifier (BaO) in glass system contributing to the highest μ_m. The higher the mass attenuation coefficient the better a particular material attenuates more photons. It was showed that the increment of BaO in the glass samples lead to an increase in the mass attenuation coefficients at 662 keV. This is because BaO increases their effective atomic numbers and densities.

Since 30BaBTe (BaO = 0.3 mol fraction) glass showed the highest density among other glasses, therefore it gave the highest mass attenuation coefficient, μ_m value. This indicated that the highest photon interaction at energy of 662 keV is occur in 30BaBTe glass. This interaction is probability through photoelectric effect and Compton scattering. There are four general situations when glass material being radiated by photons from gamma ray: (1) photons penetrates glass but no interaction occurs, (2) photons is absorbed directly into atoms in the glass structure through photoelectric effect, (3) photon interact with the glass through Compton scattering and penetrates glass, and (4) atoms interact with photons through Compton effects for several times and finally absorbed by photoelectric effect [30]. Saeed et al. 2014 [31] reported μ_m of 0.0749 cm^2/g for borate glass with 30 mol % of BaO is higher than present glass (μ_m = 0.0491 cm^2/g).

The effectiveness of gamma shielding can also be defined in terms of the half value layer and mean free path. Material with lower value of half value layer and mean free path can produce better shielding material. Half value layer is the thickness of the material needed to absorb 50 % of the incident radiation, whereas mean free path is the average distance travelled by the photon between two successive interactions. The values of mean free path (MFP) and half value layer (HVL) for all glasses are provided in Table 2 and also plotted in Figure 6. The HVL and MFP values of $[(TeO_2)_{0.7}(B_2O_3)_{0.3}]_{1-x}(BaO)_x$ glasses the HVL and MFP values are slowly decrease with increasing of glass modifier (BaO). The decreasing pattern of HVL and MFP values for $[(TeO_2)_{0.7}(B_2O_3)_{0.3}]_{1-x}(BaO)_x$ glasses are attributed to the increment in density and the mass attenuation coefficient of glasses. It is observed that the HVL and MFP for 30BaBTe glass is higher than ordinary concrete [32].

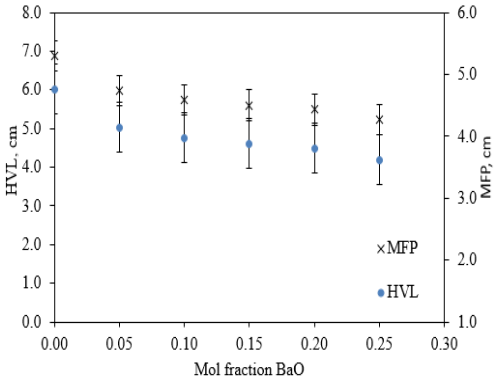

Fig. 6. Variation of HVL and MFP for $[(TeO_2)_{0.7}(B_2O_3)_{0.3}]_{1-x}(BaO)_x$ glasses.

4. Conclusion

In the present work, addition of a glass modifier, BaO, in boro-tellurite glass increased the density of the glass system. The structural properties of the glass system also changed because of increasing number of NBOs in the glass structure. The glasses with highest BaO content (x = 0.30 mol fraction) were found to give the highest mass attenuation coefficient and also have the lowest mean free path and half value layer compared other glass samples. The result of this glass sample is even better than ordinary concrete.

Acknowledgements

The authors appreciate the financial support for the work from the Ministry of Higher Education of Malaysia under FRGS grant no. FRGS/1/2013/SG06/UPNM/03/1.

References

[1] Khanna, S. S. Bhatti, K. J. Singh, K. S. Thind, Nuclear Instruments and Methods in Physics Research B **114**, 217 (1996).
[2] IPCS, Barium and barium compounds., World Health Organization, International Programme on Chemical Safety (Concise International Chemical Assessment Document 33), Geneva, (2001).
[3] WHO, Barium in drinking-water. Background document for preparation of WHO Guidelines for drinking-water quality. Geneva, World Health Organization (WHO/SDE/WSH/03.04/76), (2003).
[4] V. P. Singh, M. E. Medhat, S. P. Shirmardi, Radiation Physics and Chemistry **106**, 255 015).
[5] K. Singh, H. Singh, V. Sharma, R. Nathuram, A. Khanna, R. Kumar, S. H. Singh, Nuclear instruments and methods in physics research section B: Beam Interactions with Materials and Atoms **194**(1), 1 (2002).
[6] P. Kaur, K. J. Singh, S. Thakur, P. Singh, B. S. Bajwa, Spectrochimica Acta Part A: Molecular and Biomolecular Spectroscopy **206**, 367 (2019).
[7] P. Vani, G. Vinitha, M. I. Sayyed, B. O. Elbashir, N. Manikandan, Journal of Non-Crystalline Solids **511**, 194 (2019).
[8] M. K. Halimah, L. Hasnimulyati, A. Zakaria, S. A. Halim, M. Ishak, A. Azuraida, Materials Science & Engineering B **226,** 158 (2017).
[9] N. Manikandan, A. Ryasnyanskiy, J. Toulouse, Journal of Non-Crystalline Solids **358**, 947 012).
[10] S. Kapoor, H. B. George, A. Betzen, Affatigato, M. Feller, Range of compositions, Journal of Non-Crystalline Solids **270**(1-3), 215 (2000).
[11] D. Warner, H. Rawson, Journal of Non-Crystalline Solids **29**(2), 231 (1978).
[12] H. Desirena, A. Schülzgen, S. Sabet, G. Ramos-Ortiz, E. De la Rosa, N. Peyghambarian, Optical Materials **31**, 784 (2009).
[13] L. Hasnimulyati, M. K. Halimah, A. Zakaria, S. A. Halim, M. Ishak, C. Eevon, Journal of Ovonic Research **12**, 291 (2016).
[14] M. K. Halimah, A. Azuraida, M. Ishak, L. Hasnimulyati, Journal of Non-Crystalline Solids **512**, 140 (2019).
[15] H. Sidek, S. Rosmawati, Z. Talib, M. K. Halimah, W. Daud, American Journal Applied Sciences **6**(8), 1489 (2009).
[16] Y. B. Saddeek, G. Y. Mohamed, H. S. Hassan, A. M. A. Mostafa, G. Abd elfadeel, Journal of Non-Crystalline Solids **419**, 110 (2015).
[17] M. S. Gaafara, I. Shaaranya, T. Alharbia, Journal of Alloys and Compounds **616**, 625 (2014).
[18] S. Rada, M. Culea, E. Culea, Journal of Non-Crystalline Solids **354**, 5491 (2008).
[19] S. A. Umar, M. K. Halimah, K. T. Chan, A. A. Latif, Journal of Non-Crystalline Solids **471**, 101(2017).
[20] N. Berwal, S. Dhankha, P. Sharma, R. S. Kundu, R. Punia, N. Kishore, Journal of Molecular Structure **1127**, 636(2017).
[21] E. S. Nurbaisyatul, K. Azman, H. Azhan, W. A.W. Razali, A. Noranizah, S. Hashim, Optic Spectroscopic **116**, 413 (2014).
[22] E. I. Kamitsos, G. D. Chryssikos, Journal of Molecular Structure **247**, 1 (1991).
[23] M. A. Khaled, H. Elzahed, S. A. Fayek, M. M. El-Ocker, Materials Chemistry Physics **37**, 329 994).
[24] E. C. Paz, J. D. M. Dias, G. H. A. Melo, T. A. Lodi, J. O. Carvalho, P. F. Façanha Filho, M. J. Barboza, F. Pedrochi, A. Steimacher, Matererial Chemistry Physics **178**, 133 (2016).

[25] V. O. Sokolov, V. G. Plotnichenko, V. V. Koltashev, Journal of Non-Crystalline Solids **355,** 1574 (2009).
[26] Gautam, A. K. Yadav, A. K. Singh, ISRN Ceramics **2012**, Article ID 428497, 17 pages (2012).
[27] K. Kaur, K. J. Singh, V. Anand, Radiation Physics Chemistry **120**, 63 (2016).
[28] R. S. Kundu, S. Dhankhar, R. Punia, K. Nanda, N. Kishore, Journal of Alloys and Compounds **587**, 66 (2014).
[29] Azuraida, M. K. Halimah, A. A. Sidek, C. A. C. Azurahanim, S. M. Iskandar, M. Ishak, A. Nurazlin, Chalcogenide Letters **12**(10), 497 (2015).
[30] M. E. Çelikbilek, A. E. Ersundua, M. I. Sayyed, G. Lakshminarayana, S. Aydın, Journal of Alloys and Compounds **714**, 278 (2017).
[31] Saeed, R. M. El-Shazly, Y. H. Elbashar, A. M. El-Azm, M. M. El-Okr, M. N. H. Comsan, A. M. Osman, A. M. Abdal-Monem, A. R. El-Sersy, Radiation Physics and Chemistry **102**, 167 014).
[32] Un, F. Demir, Applied Radiation and Isotopes **80**, 73 (2013).